Inorg. Chem. **2005**, *44*, 9704–9713

Electronic Structure Study of Seven-Coordinate First-Row Transition Metal Complexes Derived from 1,10-Diaza-15-crown-5: A Successful Marriage of Theory with Experiment

Carlos Platas-Iglesias,[†] Lea Vaiana,[†] David Esteban-Gómez,[†] Fernando Avecilla,[†] José Antonio Real,[‡] Andrés de Blas,*[,†] and Teresa Rodríguez-Blas*[,†]

Departamento de Química Fundamental, Universidade da Coruña, Campus da Zapateira s/n, 15071 A Coruña, Spain, and Departament de Química Inorgánica, Doctor Moliner 50, Universitat de València, 46100 Burjassot, València, Spain

Received July 6, 2005

A detailed study of the electronic structure of seven-coordinate Mn(II), Co(II), and Ni(II) complexes with the lariat ether *N*,*N*′-bis(2-aminobenzyl)-1,10-diaza-15-crown-5 (**L**[1]) is presented. These complexes represent new examples of structurally characterized seven-coordinate (pentagonal bipyramidal) complexes for the Mn(II), Co(II), and Ni(II) ions. The X-ray crystal structures of the Mn(II) and Co(II) complexes show C_2 symmetries for the $[M(\mathbf{L}^1)]^{2+}$ cations, whereas the structures of the Ni(II) complexes show a more distorted coordination environment. The magnetic properties of the Mn(II) complex display a characteristic Curie law, whereas those of the Co(II) and Ni(II) ions show the occurrence of zero-field splitting of the $S = 3/2$ and 1 ground states, respectively. Geometry optimizations of the $[M(\mathbf{L}^1)]^{2+}$ systems (M = Mn, Co, or Ni) at the DFT (B3LYP) level of theory provide theoretical structures in good agreement with the experimental data. Electronic structure calculations predict a similar ordering of the metal-based β spin frontier MO for the Mn(II) and Co(II) complexes. This particular ordering of the frontier MO leads to a pseudodegenerate ground state for the d^8 Ni(II) ion. The distortion of the C_2 symmetry in $[Ni(\mathbf{L}^1)]^{2+}$ is consistent with a Jahn–Teller effect that removes this pseudodegeneracy. Our electronic structure calculations predict that the binding strength of **L**[1] should follow the trend Co(II) $\approx$ Mn(II) > Ni(II), in agreement with experimental data obtained from spectrophotometric titrations.

Introduction

As is well-known, the most commonly occurring coordination numbers for first-row transition metal complexes are four, five, and six, and so they have been the aim of a great variety of electronic and structural studies to date. However, the great development of the homogeneous catalysis field, particularly during recent years, has begun to focus the aim of some chemists toward first-row transition metal complexes with lower and higher coordination numbers. To deeply understand the structural features, stabilities, and/or electronic properties for these types of complexes with unusual coordination numbers, we must carry out detailed electronic structure studies. Whereas such kinds of studies have been reported recently for three-coordinate iron, cobalt, and nickel complexes,[1,2] few related studies for complexes with coordination numbers higher than six have been reported. A qualitative study of seven-coordinate complexes based on extended Hückel calculations was reported by Hoffmann et al.[3] In the present contribution, we disclose the first detailed electronic structure study of seven-coordinate first-row transition metal complexes.

Interest in heptacoordination has experienced a resurgence in recent years because the complexes are interesting as intermediates in associative reactions of six-coordinate complexes.[4] Furthermore, a few active centers in metalloproteins, such as manganese atoms in glutamine synthetase, seem to be heptacoordinate.[5] Seven-coordinate Mn(II) com-

* To whom correspondence should be addressed. E-mail: mayter@udc.es.
[†] Universidade da Coruña.
[‡] Universitat de València.

(1) Palacios, A. A.; Alemany, P.; Alvarez, S. *Inorg. Chem.* **1999**, *38*, 707−715.
(2) Holland, P. L.; Cundari, T. R.; Perez, L. L.; Eckert, N. A.; Lachicotte, R. J. *J. Am. Chem. Soc.* **2002**, *124*, 14416−14424.
(3) Hoffmann, R.; Beier, B. F.; Muetterties, E. L.; Rossi, A. R. *Inorg. Chem.* **1977**, *16*, 511−522.
(4) Atwood, J. R. *Inorganic and Organometallic Reaction Mechanisms*; Wiley-VCH: New York, 1997.

10.1021/ic051119h CCC: $30.25
Published on Web 11/15/2005

Chart 1

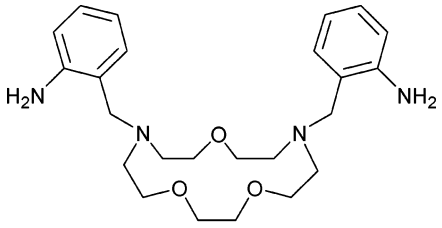

L¹

plexes that mimic the activity of superoxide dismutase have broad potential as therapeutic agents in the treatment of numerous diseases ranging from acute and chronic inflammation to cardiovascular diseases and cancer.[6] However, a recent estimate based on the number of transition metal σ-bonded complexes found in the Cambridge Structural Database reveals that heptacoordinate complexes represent 1.8% of the total number of structures reported.[7] The distribution of heptacoordination throughout the first metal transition series is also quite irregular; heptacoordination appears to be, for instance, more common for Mn and Co[8−11] than for Ni.[12] Several strategies have been designed for obtaining seven-coordinate complexes of first-row transition metals, including the use of planar[13] or macrocyclic pentadentate ligands[14] and the use of acyclic ligands that stabilize the pentagonal bipyramid by $\pi-\pi$ stacking interactions.[15] More recently, several seven-coordinate complexes of this type have been synthesized by using acyclic heptadentate ligands.[8,9] In a recent work, we demonstrated that the lariat ether *N*,*N*′-bis(2-aminobenzyl)-1,10-diaza-15-crown-5 (**L¹**, Chart 1) forms mononuclear complexes with copper(II) in which the metal ion is seven-coordinate in a distorted (axially compressed) pentagonal bipyramidal geometry.[16] Because of this, this receptor was selected to force heptacoordination in the Mn(II), Co(II), and Ni(II) complexes reported here.

To understand the structural features and electronic properties of these systems, we turned to theory. The accurate calculation of the electronic structure of transition metal complexes remains a challenging task for quantum chemistry. Although both Hartree−Fock and DFT calculations have been used for this purpose, the latter has certain advantages over the former.[17] In the DFT method, correlation is partly taken into account by considering the functional form of the exchange-correlation contribution. Thus, DFT appears to be an excellent approach for optimizing the geometries and exploring the electronic structure of systems containing first-row transition metals. However, although DFT calculations have been widely applied to the study of the electronic structure of many first-row transition metal complexes,[1,18−20] analogous studies on seven-coordinate Mn(II), Co(II), or Ni(II) metal complexes have been restricted to only aquo complexes.[21] With this in mind, we performed a theoretical study of the $[M(\mathbf{L^1})]^{2+}$ systems (M = Mn, Co, or Ni) at the DFT (B3LYP) computational level. The calculated geometries obtained from geometry optimizations were compared with the experimental structures obtained by X-ray diffraction analyses. Likewise, a molecular orbital analysis has been performed on the calculated structures to gain insight into the electronic structure of this family of complexes.

The Jahn−Teller effect states, according to its original formulation, that a nonlinear, symmetric molecule with an orbitally degenerate electronic state is unstable and gets distorted, thereby removing the electronic degeneracy, until a nondegenerate ground state is achieved.[22] The Jahn−Teller effect involves the coupling of the electronic and vibrational motions of the molecule.[23] Only certain systems are subject to Jahn−Teller distortion, depending on the number and spin state of their valence electrons and on their coordination number. Octahedral d^4 and d^9 transition metal complexes are typical examples. The Jahn−Teller theorem also predicts that a regular stereochemistry is unstable for four-coordinate tetrahedral[24] and seven-coordinate pentagonal bipyramidal high-spin nickel(II) complexes.[12] A few examples of solid-state structures of pentagonal bipyramidal high-spin nickel(II) complexes have been reported to date,[12,25] because heptacoordination is particularly rare for Ni(II). Large distortions are normally observed for these complexes,[12] which have been attributed to the Jahn−Teller effect. Nonetheless, to the best of our knowledge, theoretical support has never been reported for the Jahn−Teller effect in

(5) Gill, H. S.; Eisenberg, D. *Biochemistry* **2001**, *40*, 1903−1912.
(6) Aston, K.; Rath, N.; Naik, A.; Slomczynska, U.; Schall, O. F.; Riley, D. P. *Inorg. Chem.* **2001**, *40*, 1779−1789.
(7) Casanova, D.; Alemany, P.; Bofia, J. M.; Alvarez, S. *Chem.−Eur. J.* **2003**, *9*, 1281−1295.
(8) Gou, S.; You, X.; Yu, K.; Lu, J. *Inorg. Chem.* **1993**, *32*, 1883−1887.
(9) Horner, O.; Girerd, J.-J.; Philouze, C.; Tchertanov, L. *Inorg. Chim. Acta* **1999**, *290*, 139−144.
(10) Baffert, C.; Romero, I.; Pecaut, J.; Llobet, A.; Deronzier, A.; Collomb, M.-N. *Inorg. Chim. Acta* **2004**, *357*, 3430−3436.
(11) Capparelli, M. V.; De Meester, P.; Goodgame, D. M. L.; Gunn, S. J.; Skapski, A. C. *Inorg. Chim. Acta* **1985**, *97*, L37−L39.
(12) Giordano, T. J.; Palenik, G. J.; Palenik, R. C.; Sullivan, D. A. *Inorg. Chem.* **1979**, *18*, 2445−2450.
(13) Nardelli, M.; Pelizzi, C.; Pelizzi, G. *Transition Met. Chem.* **1977**, *2*, 35−40.
(14) Drew, M. G. B.; bin Toman, A. H.; McFall, S. G.; McIlroy, P. D. A.; Nelson, S. M. *J. Chem. Soc., Dalton Trans.* **1977**, 1173−1180.
(15) Seitz, M.; Kaiser, A.; Stempfhuber, S.; Zabel, M.; Reiser, O. *Inorg. Chem.* **2005**, *44*, 4630−4636.
(16) Rodríguez-Infante, C.; Esteban, D.; Avecilla, F.; de Blas, A.; Rodríguez-Blas, T.; Mahía, J.; Macedo, A. L.; Geraldes, C. F. G. C. *Inorg. Chim. Acta* **2001**, *317*, 190−198.
(17) Foresman, J. B.; Frisch, A. E. *Exploring Chemistry with Electronic Structure Methods*, 2nd ed.; Gaussian Inc.: Pittsburgh, PA, 1996; Chapter 6.
(18) Detrich, J. L.; Konecny, R.; Vetter, W. M.; Doren, D.; Rheingold, A. L.; Theopold, K. H. *J. Am. Chem. Soc.* **1996**, *118*, 1703−1712.
(19) Schmiedekamp, A. M.; Ryan, M. D.; Deeth, R. J. *Inorg. Chem.* **2002**, *41*, 5733−5743.
(20) Bachler, V.; Olbrich, G.; Neese, F.; Wieghardt, K. *Inorg. Chem.* **2002**, *41*, 4179−4193.
(21) Tsutsui, Y.; Wasada, H.; Funahashi, S. *Bull. Chem. Soc. Jpn.* **1998**, *71*, 73−78.
(22) Jahn, H. A.; Teller, E. *Proc. R. Soc. London, Ser. A* **1937**, *161*, 220−235.
(23) Bersuker, I. B. *Chem. Rev.* **2001**, *101*, 1067−1114.
(24) Wilk, A.; Hichman, M. A.; Massa, W.; Reinen, D. *Inorg. Chem.* **1993**, *32*, 2483−2490.
(25) (a) Carcelli, M.; Ianelli, S.; Mavilla, L.; Pelizzi, C.; Pelizzi, G. *Inorg. Chim. Acta* **1996**, *245*, 43−49. (b) Ianelli, S.; Pelizzi, C.; Pelizzi, G.; Tarasconi, P. *J. Chem. Crystallogr.* **1996**, *26*, 185−201. (c) Constable, E. C.; Lewis, J.; Liptrot, M. C.; Raithby, P. R.; Schroeder, M. *Polyhedron* **1983**, *2*, 301−302. (d) Constable, E. C.; Lewis, J.; Liptrot, M. C.; Raithby, P. R. *J. Chem. Soc., Dalton Trans.* **1984**, 2177−2185.

pentagonal bipyramidal high-spin nickel(II) complexes from quantum mechanical calculations.

Experimental Section

Chemicals and Starting Materials. All chemicals were purchased from commercial sources, and used without further purification. Solvents were of reagent grade purified by the usual methods. *N*,*N*′-Bis(2-aminobenzyl)-1,10-diaza-15-crown-5 (**L¹**) was prepared as previously described.[16]

Caution: *Although we have experienced no difficulties with the perchlorate salts, these should be regarded as potentially explosive and handled with care.*[26]

Preparation of the Complexes. [Mn(L¹)](NO₃)₂·H₂O (1). A mixture of **L¹** (0.100 g, 0.233 mmol) and $Mn(NO_3)_2{\cdot}4H_2O$ (0.060 g, 0.240 mmol) in acetonitrile (20 mL) was stirred and heated to reflux over a period of 6 h. Slow diffusion of diethyl ether into the former solution at room temperature produced colorless crystals that were collected by filtration and air-dried (yield 0.093 g, 64%). Anal. Calcd for $C_{24}H_{38}MnN_6O_{10}$: C, 46.08; H, 6.12; N, 13.43. Found: C, 46.05; H, 6.22; N, 13.42. Λ_M (acetonitrile, $cm^2\ \Omega^{-1}\ mol^{-1}$): 219 (2:1 electrolyte). IR (KBr): 3274, 3227, 3148, 3103 ($\nu(NH_2)$), 1620, ($\delta(NH_2)$), 1589 ($\nu(C{=}C)$), 1384 (NO_3^-) cm^{-1}. FAB-MS (*m*/*z* (%BPI)): 545 (29) $[Mn(\mathbf{L^1})(NO_3)]^+$, 482 (100) $[Mn(\mathbf{L^1})]^+$. Single crystals of formula $[Mn(\mathbf{L^1})](NO_3)_2{\cdot}2CH_3CN$ suitable for X-ray diffraction were grown by slow diffusion of diethyl ether into solutions of the complex in acetonitrile.

[Mn(L¹)](ClO₄)₂ (2). The preparation of the white complex followed the same procedure as that for **1** by using **L¹** (0.051 g, 0.119 mmol) and $Mn(ClO_4)_2{\cdot}6H_2O$ (0.043 g, 0.119 mmol) in 15 mL of acetonitrile (yield 0.039 g, 48%). Anal. Calcd for $C_{24}H_{36}Cl_2MnN_4O_{11}$: C, 42.24; H, 5.32; N, 8.21. Found: C, 42.40; H, 5.26; N, 8.17. Λ_M (acetonitrile, $cm^2\ \Omega^{-1}\ mol^{-1}$): 336 (2:1 electrolyte). IR (KBr): 3310, 3277 ($\nu(NH_2)$), 1618 ($\delta(NH_2)$), 1593 ($\nu(C{=}C)$), 1092 ($\nu_{as}(Cl{-}O)$), 620 ($\delta_{as}(O{-}Cl{-}O)$) cm^{-1}. FAB-MS (*m*/*z* (%BPI)): 582 (70) $[Mn(\mathbf{L^1})(ClO_4)]^+$, 482 (99) $([Mn(\mathbf{L^1})]^+)$.

[Co(L¹)](NO₃)₂·CH₃CN (3). The preparation of the pink complex followed the same procedure as that for **1** by using **L¹** (0.100 g, 0.233 mmol) and $Co(NO_3)_2{\cdot}6H_2O$ (0.072 g, 0.247 mmol) in 20 mL of acetonitrile (yield 0.090 g, 69%). Anal. Calcd for $C_{26}H_{39}CoN_7O_9$: C, 47.85; H, 6.09; N, 15.52. Found: C, 47.44; H, 6.09; N, 15.52. Λ_M (acetonitrile, $cm^{-1}\ \Omega^{-1}\ mol^{-1}$): 221 (2:1 electrolyte). IR (KBr): 3242, 3128 ($\nu(NH_2)$), 1621 ($\delta(NH_2)$), 1591 ($\nu(C{=}C)$), 1384 (NO_3^-) cm^{-1}. FAB-MS (*m*/*z* (%BPI)): 549 (11) $[Co(\mathbf{L^1})(NO_3)]^+$, 486 (100) $[Co(\mathbf{L^1})]^+$. Single crystals of formula $[Co(\mathbf{L^1})](NO_3)_2{\cdot}2CH_3CN$ suitable for X-ray diffraction were grown by slow diffusion of diethyl ether into solutions of the complex in acetonitrile.

[Co(L¹)](ClO₄)₂ (4). A mixture of **L¹** (0.100 g, 0.233 mmol) and $Co(ClO_4)_2{\cdot}6H_2O$ (0.085 g, 0.232 mmol) in absolute ethanol (22 mL) was stirred and heated to reflux for a period of 9 h. The pink precipitate that formed was isolated by filtration and air-dried (yield 0.141 g, 88%). Anal. Calcd for $C_{24}H_{36}Cl_2CoN_4O_{11}$: C, 42.00; H, 5.29; N, 8.16. Found: C, 41.99; H, 5.04; N, 8.22. Λ_M (acetonitrile, $cm^2\ \Omega^{-1}\ mol^{-1}$): 290 (2:1 electrolyte). IR (KBr): 3342, 3270 ($\nu(NH_2)$), 1618 ($\delta(NH_2)$), 1084 ($\nu_{as}(Cl{-}O)$), 622 ($\delta_{as}(O{-}Cl{-}O)$) cm^{-1}. FAB-MS (*m*/*z* (%BPI)): 586 (53) $[Co(\mathbf{L^1})(ClO_4)]^+$, 486 (100) $[Co(\mathbf{L^1})]^+$.

[Ni(L¹)](NO₃)₂·H₂O (5). The preparation of the green complex followed the same procedure as that for **1** by using **L¹** (0.051 g, 0.119 mmol) and $Ni(NO_3)_2{\cdot}6H_2O$ (0.034 g, 0.115 mmol) in 12 mL of acetonitrile (yield 0.038 g, 53%). Anal. Calcd for $C_{24}H_{38}NiN_6O_{10}$: C, 45.81; H, 6.09; N, 13.35. Found: C, 45.70; H, 6.10; N, 13.34. Λ_M (acetonitrile, $cm^2\ \Omega^{-1}\ mol^{-1}$): 198 (2:1 electrolyte). IR (KBr): 3286, 3218, 3136, 3063 ($\nu(NH_2)$), 1621 ($\delta(NH_2)$), 1592 ($\nu(C{=}C)$), 1384 (NO_3^-) cm^{-1}. FAB-MS (*m*/*z* (%BPI)): 485 (100) $[Ni(\mathbf{L^1})]^+$. Single crystals of formula $[Ni(\mathbf{L^1})](NO_3)_2{\cdot}H_2O$ suitable for X-ray diffraction were grown by slow diffusion of diethyl ether into solutions of the complex in acetonitrile.

[Ni(L¹)](ClO₄)₂ (6). A mixture of **L¹** (0.080 g, 0.186 mmol) and $Ni(ClO_4)_2{\cdot}6H_2O$ (0.070 g, 0.192 mmol) in absolute ethanol (15 mL) was stirred and heated to reflux for a period of 9 h. The green precipitate formed was isolated by filtration and air-dried (yield 0.152 g, 90%). Anal. Calcd for $C_{24}H_{36}Cl_2N_4NiO_{11}$: C, 42.01; H, 5.29; N, 8.17. Found: C, 42.03; H, 5.31; N, 8.27. Λ_M (acetonitrile, $cm^2\ \Omega^{-1}\ mol^{-1}$): 272 (2:1 electrolyte). IR (KBr): 3337, 3301, 3258, 3225 ($\nu(NH_2)$), 161 ($\delta(NH_2)$), 1590 ($\nu(C{=}C)$), 1087 ($\nu_{as}(Cl{-}O)$), 621 ($\delta_{as}(O{-}Cl{-}O)$) cm^{-1}. FAB-MS (*m*/*z* (%BPI)): 585 (59) $[Ni(\mathbf{L^1})(ClO_4)]^+$, 485 (100) $[Ni(\mathbf{L^1})]^+$. Single crystals of formula $[Ni(\mathbf{L^1})](ClO_4)_2$ suitable for X-ray diffraction were grown by slow diffusion of diethyl ether into solutions of the complex in acetonitrile.

Physical Measurements. Elemental analyses were carried out on a Carlo Erba 1108 elemental analyzer. FAB mass spectra were recorded using a FISONS QUATRO mass spectrometer with a Cs ion gun and 3-nitrobenzyl alcohol as the matrix. IR spectra were recorded, as KBr disks, using a Bruker Vector 22 spectrophotometer. Conductivity measurements were carried out at 20 °C with a Crison Micro CM 2201 conductimeter using 10^{-3} M solutions of the complexes in acetonitrile. UV−vis spectra were recorded on a Hewlett-Packard 8452A spectrophotometer with a quartz cell (path length: 10 cm). The cell holder was thermostated at 25.0 °C through circulating water. Spectrophotometric titrations were performed at 25 °C on 5×10^{-6} M solutions of **L¹** in MeCN (polarographic grade). Typically, aliquots of a fresh perchlorate salt standard solution of the envisaged metal ion (Mn(II), Co(II), Ni(II)) were added, and the UV−vis spectra of the samples were recorded. All spectrophotometric titration curves were fitted with the HYPERQUAD program.[27] Variable-temperature magnetic susceptibility measurements were carried out using microcrystalline samples (20−60 mg) of compounds **1**, **3**, **4**, and **5**, using a Quantum Design MPMS2 SQUID susceptometer equipped with a 5.5 T magnet, operating at 0.1−0.5 T and at temperatures from 300 to 1.8 K. The susceptometer was calibrated with $(NH_4)_2Mn(SO_4)_2{\cdot}12H_2O$. Experimental susceptibilities were corrected for diamagnetism of the constituent atoms by the use of Pascal's constants.

Crystal Structure Determinations. Crystal data and details on data collection and refinement are summarized in Table 1. Three-dimensional X-ray data were collected on a Bruker SMART 1000 CCD difractometer by the $\phi-\omega$ scan method. Reflections were measured from a hemisphere of data collected of frames each covering 0.3° in ω. Of the 9517, 9149, 34 035, and 18 756 reflections measured for complexes **1**, **3**, **5**, and **6**, all of which were corrected for Lorentz and polarization effects and for absorption by semiempirical methods on the basis of symmetry-equivalent and repeated reflections, 1457, 2355, 4244, and 4267 independent reflections, respectively, exceeded the significance level $|F|/\sigma|F| > 4.0$. Complex scattering factors were taken from the program package SHELXTL,[28] as implemented on a Pentium computer. The structures were solved by direct methods and refined by full-matrix least-squares methods on F^2. The hydrogen atoms

(26) Wolsey, W. C. *J. Chem. Educ.* **1973**, *50*, A335−A337.
(27) Gans, P.; Sabatini, A.; Vacca, A. *Talanta* **1996**, *43*, 1739−1753.
(28) Sheldrick, G. M. *SHELXTL*, version 5.1; Bruker AXS: Madison, WI, 1997.

Table 1. Crystal and Structure Refinement Data for Compounds **1**, **3**, **5**, and **6**

	1	**3**	**5**	**6**
formula	$C_{28}H_{42}MnN_8O_9$	$C_{28}H_{42}CoN_8O_9$	$C_{24}H_{38}N_6NiO_{10}$	$C_{24}H_{36}Cl_2N_4NiO_{11}$
mol wt	689.64	693.63	629.31	686.18
space group	*C*2/*c*	*C*2/*c*	Pbca	$P2_1/c$
cryst syst	monoclinic	monoclinic	orthorhombic	monoclinic
a (Å)	12.225(2)	12.252(17)	15.8519(15)	18.122(4)
b (Å)	16.126(3)	16.22(2)	12.5941(12)	12.746(4)
c (Å)	16.872(3)	16.97(2)	28.328(3)	12.378(4)
β (deg)	91.996(4)	92.40(2)	90	92.354(17)
V (Å^3)	3324.1(11)	3370(8)	5655.5(9)	2856.6(13)
Z	4	4	8	4
T (K)	293(2)	298(2)	298(2)	298(2)
Mo Kα, λ (Å)	0.71073	0.71073	0.71073	0.71073
D_{calc} (g cm^{-3})	1.378	1.367	1.478	1.596
μ (mm^{-1})	0.459	0.571	0.751	0.933
R_{int}	0.0688	0.0316	0.0328	0.0455
R_1[a]	0.0610	0.0515	0.0567	0.0572
wR_2 (all data)[b]	0.2066	0.1582	0.1849	0.1435

[a] $R_1 = \sum||F_0| - |F_c||/\sum|F_0|$. [b] $wR_2 = \{\sum[w(|F_0|^2 - |F_c|^2|)^2]/\sum[w(F_0^4)]\}^{1/2}$.

were included in calculated positions and refined by using a riding mode, except the hydrogen atoms H1N and H2N for **1**; H2A and H2B for **3**; H3A, H3B, H4A, and H4B for **5**; and H3A, H3B, H4A, and H4B for **6**, which were left to refine freely. Refinement converged with allowance for thermal anisotropy of all non-hydrogen atoms in all compounds.

Computational Methods. The $[M(\mathbf{L^1})]^{2+}$ (M = Mn, Co, or Ni) systems were fully optimized in vacuo by using the UB3LYP density functional model.[29,30] The X-ray crystal structures of compounds **1**, **3**, and **5** were used as input for geometry optimizations. In these calculations, we used a mixed basis set, comprising the standard 6-31G(d) basis on N and O atoms, the 3-21G basis on C and H atoms, and Ahlrichs' valence triple-ζ (VTC) on the metal atoms.[31] For the $[Co(\mathbf{L^1})]^{2+}$ and $[Ni(\mathbf{L^1})]^{2+}$ systems, both high-spin (Co: $S = 3/2$; Ni: $S = 1$) and low-spin (Co: $S = 1/2$; Ni: $S = 0$) situations were modeled, whereas for $[Mn(\mathbf{L^1})]^{2+}$ high-spin ($S = 5/2$), low-spin ($S = 1/2$), and intermediate-spin ($S = 3/2$) configurations were taken into account. The stationary points found on the potential-energy surfaces as a result of the geometry optimizations have been tested to represent energy minima rather than saddle points via frequency analysis. On the optimized structures, single-point energy calculations were also performed by using the pure UBLYP density functional model. In vacuo relative free energies of the different spin configurations of the $[M(\mathbf{L^1})]^{2+}$ systems with respect to the high-spin configuration were calculated at the B3LYP and BLYP levels, and they include nonpotential energy contributions (that is, zero-point energy and thermal terms) obtained by frequency analysis. The $[Ni(\mathbf{L^1})]^{2+}$ system was studied by the potential-energy surface scan using the UB3LYP model. The Ni(1)−O(2) distance was varied in steps of 0.04 Å between 2.087 and 2.527 Å, generating 12 points. All UDFT calculations were performed by using the Gaussian 98 package (revision A.11.3).[32] Percentage compositions of molecular orbitals were calculated using the AOMix program.[33,34]

Results and Discussion

X-ray Crystal Structures. The solid-state structures of compounds **1**, **3**, **5**, and **6** were determined by single-crystal X-ray diffraction analyses. Crystals contain the cations $[M(\mathbf{L^1})]^{2+}$ (M = Mn, Co, or Ni) and nitrate or perchlorate anions. Some of these anions are involved in hydrogen-bonding interactions with the aniline groups (Table S1, Supporting Information). Compounds **1** and **3** crystallize in the *C*2/*c* monoclinic space group, and the asymmetric unit contains a half-molecule. Table 2 summarizes selected bond lengths for compounds **1** and **3**, whereas the structures of the $[M(\mathbf{L^1})]^{2+}$ cations (M = Mn or Co) are depicted in Figure 1. The Ni(II) complexes **5** and **6** crystallize in the orthorhombic *Pbca* and monoclinic $P2_1/c$ space groups, respectively. The structures of the $[Ni(\mathbf{L^1})]^{2+}$ cations in **5** and **6** are shown in Figure 2, whereas selected bond lengths and angles are given in Table 2. The $[Ni(\mathbf{L^1})]^{2+}$ cations in **5** and **6** show significantly different bond distances of the Ni(II) coordination environment. Therefore, the nature of the counterion (nitrate or perchlorate) appears to have an effect on the structure of the cation, even when the anions remain noncoordinated. Every complex cation $[M(\mathbf{L^1})]^{2+}$ (M = Mn, Co, or Ni) contains a MN_4O_3 core with the seven heteroatoms of $\mathbf{L^1}$ coordinated to the metal ion. The cations present in **1** and **3** show a slightly distorted C_2 symmetry, whereas the $[Ni(\mathbf{L^1})]^{2+}$ cations in **3** and **4** present C_1 symmetry. The metal ion is placed in the macrocyclic cavity bound to the three ether oxygen atoms and the two pivotal nitrogen atoms. The donor atoms of the pendant arms coordinate apically. The bibracchial lariat ether $\mathbf{L^1}$ shows an anti arrangement with both pendant arms pointing to opposite sides of the crown moiety. These results contrast with the solid-state structures

(29) Becke, A. D. *J. Chem. Phys*. **1993**, *98*, 5648−5652.
(30) Lee, C.; Yang, W.; Parr, R. G. *Phys. Rev. B* **1988**, *37*, 785−789.
(31) Schäefer, A.; Horn, H.; Ahlrichs, R. *J. Chem. Phys*. **1992**, *97*, 2571−2577.
(32) Frisch, M. J.; Trucks, G. W.; Schlegel, H. B.; Scuseria, G. E.; Robb, M. A.; Cheeseman, J. R.; Zakrzewski, V. G.; Montgomery, J. A., Jr.; Stratmann, R. E.; Burant, J. C.; Dapprich, S.; Millam, J. M.; Daniels, A. D.; Kudin, K. N.; Strain, M. C.; Farkas, O.; Tomasi, J.; Barone, V.; Cossi, M.; Cammi, R.; Mennucci, B.; Pomelli, C.; Adamo, C.; Clifford, S.; Ochterski, J.; Petersson, G. A.; Ayala, P. Y.; Cui, Q.; Morokuma, K.; Malick, D. K.; Rabuck, A. D.; Raghavachari, K.; Foresman, J. B.; Cioslowski, J.; Ortiz, J. V.; Baboul, A. G.; Stefanov, B. B.; Liu, G.; Liashenko, A.; Piskorz, P.; Komaromi, I.; Gomperts, R.; Martin, R. L.; Fox, D. J.; Keith, T.; Al-Laham, M. A.; Peng, C. Y.; Nanayakkara, A.; Challacombe, M.; Gill, P. M. W.; Johnson, B.; Chen, W.; Wong, M. W.; Andres, J. L.; Gonzalez, C.; Head-Gordon, M.; Replogle, E. S.; Pople, J. A. *Gaussian 98*, revision A.11; Gaussian, Inc.: Pittsburgh, PA, 1998.
(33) Gorelsky, S. I. *AOMix Program for Molecular Orbital Analysis*, revision 5.73; http://www.sg-chem.net/aomix/; York University: Toronto, ON, 1997.
(34) Gorelsky, S. I.; Lever, A. B. P. *J. Organomet. Chem.* **2001**, *635*, 187−196.

Table 2. Selected Experimental (X-ray) Bond Lengths (Å) of the Metal Coordination Environment in Crystalline $[M(\mathbf{L^1})]^{2+}$ Complexes (M = Mn, Co, or Ni) Compared with the Corresponding Theoretical Optimized Values

$[Mn(\mathbf{L^1})]^{2+}$

	X-ray (**1**)	calcd
Mn(1)−O(2A)	2.218(4)	2.266
Mn(1)−O(2)	2.218(4)	2.267
Mn(1)−O(1)	2.231(6)	2.251
Mn(1)−N(2)	2.303(4)	2.313
Mn(1)−N(2A)	2.303(4)	2.313
Mn(1)−N(1)	2.332(4)	2.384
Mn(1)−N(1A)	2.332(4)	2.385
AF_i[a]	0.017	

$[Co(\mathbf{L^1})]^{2+}$

	X-ray (**3**)	calcd
Co(1)−O(2A)	2.214(3)	2.259
Co(1)−O(2)	2.214(3)	2.259
Co(1)−O(1)	2.249(5)	2.243
Co(1)−N(2)	2.192(4)	2.165
Co(1)−N(2A)	2.192(4)	2.165
Co(1)−N(1)	2.274(4)	2.331
Co(1)−N(1A)	2.274(4)	2.330
AF_i[a]	0.019	

$[Ni(\mathbf{L^1})]^{2+}$

	X-ray (**5**)	X-ray (**6**)	calcd
Ni(1)−O(1)	2.467(3)	2.554(3)	2.594
Ni(1)−O(2)	2.438(3)	2.331(2)	2.247
Ni(1)−O(3)	2.044(3)	2.064(2)	2.110
Ni(1)−N(1)	2.245(3)	2.309(3)	2.402
Ni(1)−N(2)	2.197(3)	2.146(3)	2.155
Ni(1)−N(3)	2.106(3)	2.100(3)	2.110
Ni(1)−N(4)	2.117(3)	2.092(3)	2.093
AF_i[a]	0.049	0.024	

[a] Agreement factor between the experimental and calculated bond distances: $AF_i = [\sum(\text{exp} - \text{calcd})^2/\sum(\text{exp})^2]^{1/2}$, where exp and calcd denote experimental and calculated values, respectively.

of the corresponding Ba(II)[35] and Pb(II)[36] complexes of $\mathbf{L^1}$, in which the receptor adopts a syn arrangement of the pendant arms as a consequence of the larger size of these metal ions. The coordination sphere of the metal ions can be described as a distorted pentagonal bipyramid whose equatorial plane is defined by the three ether oxygen atoms and the two pivotal nitrogen atoms. The mean deviation from planarity of the plane containing the five equatorial donor atoms and the metal ion is small, and amounts to 0.1387 Å in **1**, 0.1302 Å in **3**, 0.2089 Å in **5**, and 0.1817 Å in **6**. Angles N(2)−M(1)−N(2A) in **1** and **3**, as well as angles N(3)−M(1)−N(4) in **5** and **6** are close to the ideal value for a regular pentagonal bipyramid (180°, see Table S1, Supporting Information). Angles D(1)−M(1)−D(2) (where D(1) and D(2) represent adjacent donor atoms of the equatorial plane) are also close to the ideal value of 72° (Table S2, Supporting Information). Finally, the vectors defined by the metal ion and the axial donors (N(2) and N(2A) in **1** and **3**, or N(3) and N(4) in **5** and **6**) form angles close to 90° with the vectors containing the metal ion and the equatorial donor

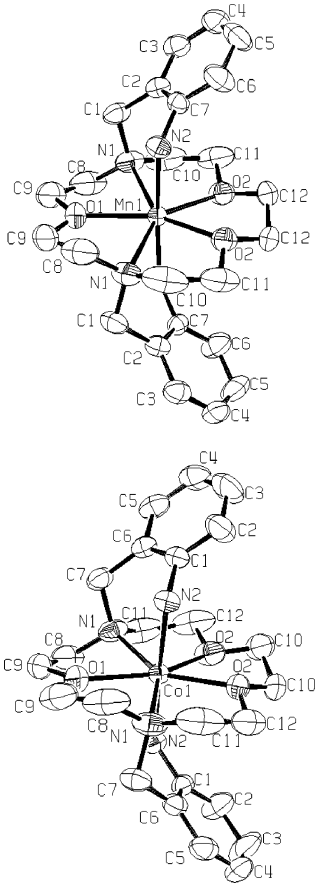

Figure 1. X-ray crystal structures of the cations in compounds **1** (top) and **3** (bottom) with atom labeling; hydrogen atoms are omitted for simplicity; the ORTEP plot is drawn at the 30% probability level.

atoms, as expected for a pentagonal bipyramidal coordination environment.

Inspection of the data reported in Table 2 reveals a more distorted polyhedron around the Ni(II) ion in **5** and **6** than around the Mn(II) or Co(II) ions in **1** and **3**. Two of the Mn(1)−O or Co(1)−O bond distances in **1** and **3** are identical (M(1)−O(2) and M(1)−O(2A)), and are very similar to the third one (M(1)−O(1), Table 2). However, this is not the case for compounds **5** and **6**, which present two long Ni−O bond distances (Ni(1)−O(1) and Ni(1)−O(2)) and a short one (Ni(1)−O(3), Table 2). This distortion of the coordination polyhedra in **5** and **6** is probably linked to the Jahn−Teller effect, which is expected to operate in seven-coordinate pentagonal bipyramidal high-spin Ni(II) complexes.[12]

Magnetic Properties. The $\chi_M T$ product (where χ_M is the molar magnetic susceptibility and T the temperature) vs T has been analyzed for **1**, **3**, **4**, and **5** in the range of temperatures 2−300 K. Figure 3 displays the $\chi_M T$ vs T plots for **1**, **3**, and **5**. For **1**, $\chi_M T$ is equal to 4.37 cm^3 K mol^{-1}, a value that remains practically independent of temperature and corresponds exactly to what it is expected to be for an isolated Mn(II) ion exhibiting a Curie law with $g = 2.00$. The magnetic behavior of **2** is expected to be the same as that of **1**. The magnetic behaviors of **3** and **4** are very similar; $\chi_M T$ is equal to 2.30 (**3**) or 2.13 (**4**) cm^3 K mol^{-1} at 300 K. These values are larger than that expected for the spin-only formula for a mononuclear high-spin Co(II) complex ($S =$

(35) Esteban, D.; Bañobre, D.; Bastida, R.; de Blas, A.; Macías, A.; Rodríguez, A.; Rodríguez-Blas, T.; Fenton, D. E.; Adams, H.; Mahía, J. *Inorg. Chem.* **1999**, *38*, 1937−1944.
(36) Esteban, D.; Bañobre, D.; de Blas, A.; Rodríguez-Blas, T.; Bastida, R.; Macías, A.; Rodríguez, A.; Fenton, D. E.; Adams, H.; Mahía, J. *Eur. J. Inorg. Chem.* **2000**, 1445−1456.

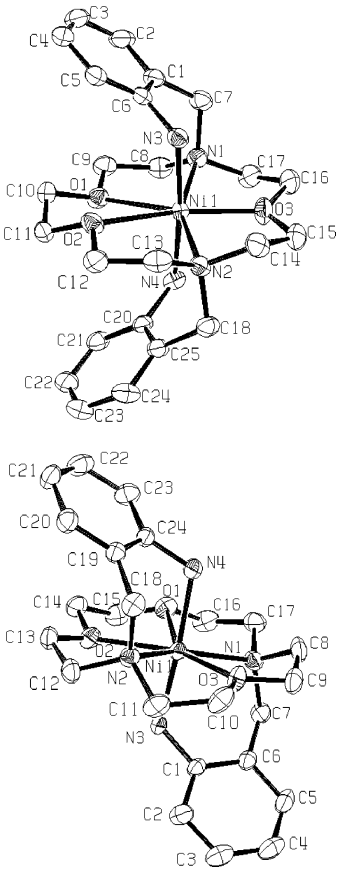

Figure 2. X-ray crystal structures of the cations in compounds **5** (top) and **6** (bottom) with atom labeling; hydrogen atoms are omitted for simplicity; the ORTEP plot is drawn at the 30% probability level.

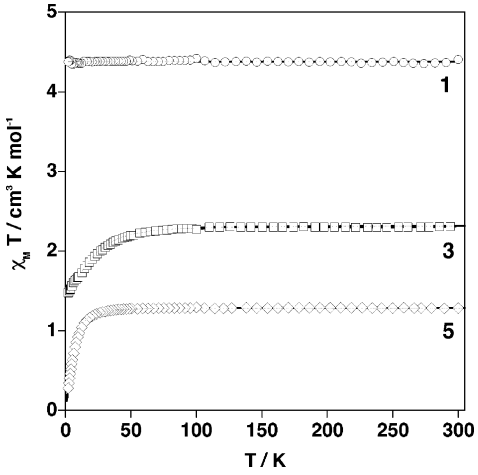

Figure 3. Magnetic properties of compounds **1**, **3**, and **5**. Solid lines represent the best fit between calculated and experimental data.

3/2), indicating that a relevant orbital contribution is involved. $\chi_M T$ remains essentially constant from room temperature down to ca. 60 K. It then decreases significantly when cooling, to reach a value of 1.47 (**3**) or 1.31 (**4**) cm^3 K mol^{-1} at 2.0 K. According to the distorted pentagonal bipyramidal coordination geometry described for **3**, the magnetic behavior of both cobalt derivatives may be associated with the occurrence of zero-field splitting of the orbitally nondegenerate $S = 3/2$ ground state of Co(II). Consequently, to account for the low-temperature region in **3** and **4**, we have considered the occurrence of an axial crystal zero-field splitting D using the Hamiltonian (eq 1) with $S = 3/2$.

$$H = D[\hat{S}_z^2 - (1/3)S(S+1)] + g\beta H\hat{S} \quad (1)$$

The following expressions for the magnetic susceptibility have been derived from eq 1

$$\chi_M = \frac{(\chi_z + 2\chi_{x,y})}{3} \quad (2)$$

$$\chi_z = \frac{Ng_z^2\beta^2}{4kT}\frac{1 + 9\exp(-2D/kT)}{1 + \exp(-2D/kT)} \quad (3)$$

$$\chi_{x,y} = \frac{Ng_{x,y}^2\beta^2}{kT}\frac{1 + (3kT/4D)[1 - \exp(-2D/kT)]}{1 + \exp(-2D/kT)} \quad (4)$$

in which all the variables have their usual meaning. The best set of parameters that matches the experimental data is found to be $D = 25$ cm^{-1} and $g_{average} = 2.22$ with $R = 4 \times 10^{-5}$ for **3**, and $D = 26$ cm^{-1} and $g_{average} = 2.15$ with $R = 8 \times 10^{-5}$ for **4**. R is the agreement factor defined as $\sum_i[(\chi_M)_i^{exptl} - [(\chi_M)_i^{calc}]^2/[(\chi_M)_i^{exptl}]^2]$. The solid line in Figure 3 corresponds to the calculated curve, showing that an excellent agreement between the experimental and theoretical $\chi_M T$ data is achieved.

The $\chi_M T$ product is ca. 1.33 cm^3 K mol^{-1} at 300 K, and remains constant down to 50 K for **5**. $\chi_M T$ decreases significantly at lower temperatures, attaining a value of 0.26 cm^3 K mol^{-1} at 2.0 K. This behavior also reflects the occurrence of zero-field splitting of the $S = 1$ ground state of the Ni(II) ion. Developing the Hamiltonian 1 for $S = 1$, we can deduce the following expressions (eqs 5 and 6) for the magnetic susceptibility

$$\chi_z = \frac{2Ng_z^2\beta^2}{kT}\frac{\exp(-D/kT)}{1 + 2\exp(-D/kT)} \quad (5)$$

$$\chi_{x,y} = \frac{2Ng_{x,y}^2\beta^2}{D}\frac{1 - \exp(-D/kT)}{1 + 2\exp(-D/kT)} \quad (6)$$

The best fit for calculated (from eq 2) and experimental χ_M values has been found for $D = 15$ cm^{-1}, $g_{x,y} = 2.27$, and $R = 1 \times 10^{-4}$. Taking into consideration that **1** displays an almost perfect Curie law in the whole range of temperature and that the crystal structures of these compounds are essentially similar, we have ruled out the occurrence of intermolecular interactions in the analysis of the magnetic data.

DFT Studies: Geometry Optimizations. To gain insight into the electronic structure of the $[M(\mathbf{L^1})]^{2+}$ systems (M = Mn, Co, or Ni), we carried out density functional theory (DFT) calculations using the unrestricted B3LYP model. Full geometry optimizations were performed in vacuo by using the standard 6-31G(d) basis on N and O atoms, the 3-21G basis on C and H atoms, and Ahlrichs' valence triple-ζ (VTC) on the metal atoms.[31] The latter basis has been shown to provide accurate molecular structures for several first-row transition metal complexes.[1] On the basis of the magnetic properties described above, we fixed the spin multiplicity

Table 3. In Vacuo Energy Differences (ΔE) between High-, Low-, and Intermediate-Spin Forms for the $[M(\mathbf{L^1})]^{2+}$ Systems (M = Mn, Co, or Ni)[a]

	basis set	high-spin	low-spin	intermediate-spin
$[Mn(\mathbf{L^1})]^{2+}$	B3LYP	0	220.77[b]	146.72
	BLYP	0	165.78[b]	96.32
$[Co(\mathbf{L^1})]^{2+}$	B3LYP	0	78.87	
	BLYP	0	36.76	
$[Ni(\mathbf{L^1})]^{2+}$	B3LYP	0	122.47	
	BLYP	0	68.33	

[a] Values in kJ mol^{-1}. [b] The wave functions show a large spin contamination.

of the Mn, Co, and Ni centers at 6, 4, and 3, respectively. The X-ray crystal structures of compounds **1**, **3**, and **5** described above were used as input geometries. In Table 2, the most relevant geometrical parameters calculated for the $[M(\mathbf{L^1})]^{2+}$ (M = Mn, Co, or Ni) systems are compared with the available X-ray data. Since geometry optimizations were performed by using an unrestricted model, spin contamination[37] was assessed by a comparison of the expected difference between $S(S+1)$ for the assigned spin state and the actual value of $\langle S^2 \rangle$.[38] Our results (Table S3, Supporting Information) indicate that spin contamination is negligible for every $[M(\mathbf{L^1})]^{2+}$ system in the high-spin situation.[19]

Geometry optimizations of the $[M(\mathbf{L^1})]^{2+}$ systems (M = Mn, Co, or Ni) were also carried out for other plausible spin multiplicities by using the UB3LYP model, to see if the computational scheme chosen is consistent with the experimental magnetic data. The calculated geometries (not discussed in this paper) are given in the Supporting Information. The degree of spin contamination of the UB3LYP wave functions for the different $[M(\mathbf{L^1})]^{2+}$ systems in intermediate- or low-spin situations was found to be negligible, except for the $[Mn(\mathbf{L^1})]^{2+}$ complex in the low-spin state. In the latter case, there is a large spin contamination in the UB3LYP wave function (Table S3, Supporting Information). The absolute energies of the high-spin, low-spin, and intermediate-spin (for $[Mn(\mathbf{L^1})]^{2+}$) complexes can be compared to determine which spin state is more stable. In all cases, the lowest-energy structure calculated by using the B3LYP functional is high-spin (Table 3), in agreement with the experimental data.

It has been demonstrated that the low-spin/high-spin energy splitting for some transition metal complexes cannot be well described by density functional methods.[39] In particular, the use of pure and hybrid functionals yields low-spin/high-spin energy differences that differ by up to 100 kJ mol^{-1}.[40] Thus, we also determined the energy differences between the different plausible spin states by using the pure BLYP functional. The results obtained from the UBLYP calculations (Table 3) predict the high-spin configuration to be the most stable one, in agreement with the experimental results. However, we find that the hybrid functional low-spin/high-spin splitting differs from the pure density functional by ca. 40−55 kJ mol^{-1}. Thus, the B3LYP hybrid functional appears to stabilize those states with higher multiplicities, whereas BLYP favors the low-spin states.

According to Table 2, the bond lengths calculated for the $[Mn(\mathbf{L^1})]^{2+}$ and $[Co(\mathbf{L^1})]^{2+}$ systems are close to those observed experimentally (within 0.06 Å), as evidenced by the excellent agreement factors obtained (Table 2, $AF_i = [\sum(\text{exp} - \text{calcd})^2/\sum(\text{exp})^2]^{1/2}$, where exp and calcd denote experimental and calculated values, respectively).[41,42] Calculated bond angles of the metal-coordination environment are also close to the experimental values (Table S2, Supporting Information). Although no geometrical constraints were used during the geometry optimization, the calculated structures correspond to nearly undistorted C_2 symmetries, in agreement with the experimental evidence. For the $[Ni(\mathbf{L^1})]^{2+}$ system, our DFT calculations provide a minimum energy geometry that presents a C_1 symmetry, also in agreement with the X-ray analysis. The calculated structure for $[Ni(\mathbf{L^1})]^{2+}$ clearly resembles the X-ray structures of compounds **5** and **6** (Table 2, see also Table S2, Supporting Information). Overall, the calculated structure shows a better agreement with the solid-state structure of the perchlorate complex **6** than with that of **5**, as evidenced by the lower AF_i agreement factors obtained (see Table 2 and Table S2, Supporting Information). Even so, the agreement between the experimental and calculated bond lengths and angles is not as good as that for the Co(II) or Mn(II) systems. To understand this, we have performed a potential-energy surface scan of the $[Ni(\mathbf{L^1})]^{2+}$ system. The Ni(1)−O(2) distance was varied in steps of 0.04 Å between 2.087 and 2.527 Å, generating 12 points. The results show that the Ni(1)−N(1) distance shortens as the Ni(1)−O(2) distance gets longer. Our calculations also show a rather shallow potential-energy surface for that motion, which complicates the problem of a precise theoretical determination of the $[Ni(\mathbf{L^1})]^{2+}$ molecular structure. For instance, a calculated geometry with bond distances of the Ni(II) coordination environment of Ni(1)−O(1) = 2.478 Å, Ni(1)−O(2) = 2.447 Å, and Ni(1)−N(1) = 2.246 Å, which are in close agreement with those distances determined experimentally for **5**, presents a relative energy with respect to the local minimum of only 0.2 kcal mol^{-1}. The shallow potential-energy surface calculated for this system is in agreement with the experimental evidence, which shows that, depending on the nature of the counterion, the Ni(1)−N(1) and Ni(1)−O(2) bond distances may be substantially different.

DFT Studies: Electronic Structure. To simplify the study of the electronic structure, we conveniently define a local coordinate system that will apply for these complexes. Accordingly, the *z* axis in the input structures is chosen such

(37) A discussion of some problems associated with the quantum mechanical treatment of open-shell molecules including the problem of spin contamination is given in the following: Stanton, J. F.; Gauss, J. *Adv. Chem. Phys.* **2003**, *125*, 101−146.
(38) Montoya, A.; Truong, T. N.; Sarofim, A. F. *J. Phys. Chem. A* **2000**, *104*, 6108−6110.
(39) Bruschi, M.; De Gioia, L.; Zampella, G.; Reiher, M.; Fantucci, P.; Stein, M. *J. Biol. Inorg. Chem.* **2004**, *9*, 873−884.
(40) Reiher, M.; Salomon, O.; Hess, B. A. *Theor. Chem. Acc.* **2001**, *107*, 48−55.
(41) Willcott, M. R.; Lenkinski, R. E.; Davis, R. E. *J. Am. Chem. Soc.* **1972**, *94*, 1742−1744.
(42) Davis, R. E.; Willcott, M. R. *J. Am. Chem. Soc.* **1972**, *94*, 1744−1745.

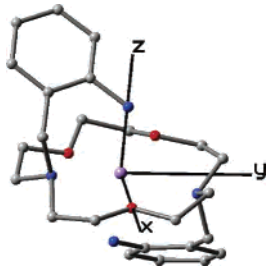

Figure 4. Definition of the coordinate system for the $[M(\mathbf{L^1})]^{2+}$ complexes used in electronic structure calculations.

that it contains one of the primary amine nitrogen atoms and the divalent metal ion placed at the origin, and the *x* axis is defined so that the M(1)−O(1) (M = Mn or Co) or M(1)−O(3) (M = Ni) vectors lie in the *x*−*z* plane (Figure 4). Electronic structure calculations yield the electronic energy and the wave function of a molecular system in a particular electronic state. The wave function itself is not very suitable for interpretation, as it is a function of the coordinates of all electrons. Thus, simplified notions and characteristics of the wave function are needed to get insight into the electronic structure of molecules. The most widely used procedure for obtaining information on electronic structure of molecules is the Mulliken population analysis (MPA).[43] It has been shown that the structural stability of seven-coordinate complexes of first-row transition metals is determined by the d electron configuration.[21] In terms of spin-unrestricted calculations, the different d electron configuration of $[M(\mathbf{L^1})]^{2+}$ complexes along the first-row transition series is reflected in the occupation of the β spin orbitals. Thus, we will focus the following discussion on the β spin orbitals. The energies and occupancies of the frontier β MO with important metal character for the $[Mn(\mathbf{L^1})]^{2+}$ and $[Co(\mathbf{L^1})]^{2+}$ systems are listed in Table 4; other orbitals are omitted for clarity. Table 4 also lists the atomic *3d* orbital contributions to the frontier β MO calculated by MPA. The orbital labels follow the usual convention for symmetry labels in C_2, except that the numbering arbitrarily begins with the lowest-energy state shown.

A quantitative molecular orbital diagram for the $[M(\mathbf{L^1})]^{2+}$ systems (M = Mn, Co) is given in Figure 5. The energies shown in Figure 5 are for the β spin orbitals containing metal character, and only the occupations for this spin state are indicated. The Mn(II) and Co(II) complexes show a similar ordering of the metal-based frontier molecular orbitals. The metal contribution to the first two β frontier MOs, $a^{(1)}$ and $b^{(1)}$, is mainly d_{yz} and d_{xz}, respectively (Table 4). These molecular orbitals are correlated with the double degenerate e_1'' orbitals in D_{5h} symmetry, and they are vacant in the case of the Mn(II) complex and occupied in $[Co(\mathbf{L^1})]^{2+}$. At somewhat higher energy are the $a^{(2)}$ and $b^{(2)}$ molecular orbitals, which possess $d_{x^2-y^2}$ and d_{xy} character, respectively (Table 4). The order of these vacant frontier orbitals, which are related to the double degenerate e_2' orbitals in D_{5h} symmetry, is interchanged between the Mn(II) and Co(II) complexes. At highest energy are the $a^{(3)}$ orbitals, whose metal contribution is primarily d_{z^2} (Table 4). The orbital ordering shown in Figure 5 confirms the qualitative view for a pentagonal bipyramidal molecular coordination presented by Hoffman et al. on the basis of extended Hückel calculations.[3]

Table 4. Irreducible Representations, Energies, and Occupancies of the Frontier β MO as Obtained from UB3LYP Calculations for the $[M(\mathbf{L^1})]^{2+}$ Complexes (M = Mn, Co, or Ni), and Contributions of d AO of the Metal (obtained by MPA)

$\Gamma(C_2)$	energy (eV)	occ	% d
		$[Mn(\mathbf{L^1})]^{2+}$	
$a^{(3)}$	−4.70	0	69.5 d_{z^2}
$b^{(2)}$	−5.32	0	67.5 d_{xy}
$a^{(2)}$	−5.37	0	74.8 $d_{x^2-y^2}$, 4.5 d_{yz}
$b^{(1)}$	−5.90	0	72.7 d_{xz}
$a^{(1)}$	−6.13	0	64.3 d_{yz}, 4.0 $d_{x^2-y^2}$
		$[Co(\mathbf{L^1})]^{2+}$	
$a^{(3)}$	−6.47	0	70.8 d_{z^2}
$a^{(2)}$	−7.39	0	68.7 $d_{x^2-y^2}$, 18.4 d_{yz}
$b^{(2)}$	−7.40	0	71.2 d_{xy}, 17.4 d_{xz}
$b^{(1)}$	−12.55	1	44.0 d_{xz}, 6.2 d_{xy}
$a^{(1)}$	−12.73	1	66.1 d_{yz}, 10.3 $d_{x^2-y^2}$
		$[Ni(\mathbf{L^1})]^{2+}$	
$a^{(3)}$ [a]	−7.50	0	73.7 d_{z^2}
$a^{(2)}$	−7.85	0	78.2 $d_{x^2-y^2}$
$b^{(2)}$	−12.69	1	17.6 d_{xy}
$b^{(1)}$	−13.70	1	31.2 d_{xz} [b]
$a^{(1)}$	−13.98	1	74.9 d_{yz}

[a] The orbital labels follow the same convention used for Mn(II) and Co(II), even when the Ni(II) complex shows a C_1 symmetry. [b] There is a second MO with less important metal d_{xy} character (18.2%) with an energy of −13.49 eV.

Surface plots of calculated frontier β spin molecular orbitals for the $[Mn(\mathbf{L^1})]^{2+}$ system are shown in Figure 6. The $a^{(3)}$ molecular orbital possesses antibonding character with respect to the interaction between the metal atom and the nitrogen donor atoms of the pendant arms and the donor atoms of the macrocyclic ligand. Figure 6 also shows that the $a^{(2)}$ and $b^{(2)}$ molecular orbitals of both molecules are antibonding with respect to the interaction between the metal and the donor atoms of the macrocyclic ligand. Finally, the $b^{(1)}$ and $a^{(1)}$ MOs possess slightly antibonding and nonbonding character, respectively. Inspection of the surface plots of calculated frontier β spin molecular orbitals for $[Co(\mathbf{L^1})]^{2+}$ leads to similar conclusions. Because of the nearly nonbonding character of the β spin $b^{(1)}$ and $a^{(1)}$ MOs, one expects the binding strengths of $\mathbf{L^1}$ to Mn(II) and to Co(II) ions to be similar.

The energies and occupancies of the frontier β MOs with important metal character for $[Ni(\mathbf{L^1})]^{2+}$ are listed in Table 4. In order to allow for correlations between the different $[M(\mathbf{L^1})]^{2+}$ complexes, we used the same conventions for the orbital labels as were used for Mn(II) and Co(II), even when the Ni(II) complex shows a C_1 symmetry. A quantitative molecular orbital diagram for $[Ni(\mathbf{L^1})]^{2+}$ is given in Figure 5. As expected from the results obtained for the Co(II) complex, the Ni contribution to the vacant $a^{(3)}$ and $a^{(2)}$ MOs is primarily d_{z^2} and $d_{x^2-y^2}$, respectively (Table 4). At lower energy is the $b^{(2)}$ MO, whose main Ni contribution is d_{xy}. The energy gap between the β $a^{(2)}$ and $b^{(2)}$ MOs is as high as 4.84 eV. Therefore, the molecular distortion in $[Ni(\mathbf{L^1})]^{2+}$ clearly removes the pseudodegeneracy of those MOs with

(43) Mulliken, R. S. *J. Chem. Phys*. **1955**, *23*, 1833−1840.

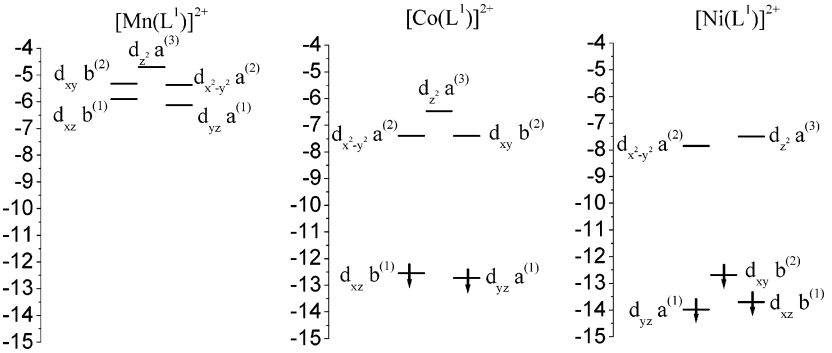

Figure 5. DFT energies (eV) of β frontier molecular orbitals in optimal geometries of $[M(\mathbf{L^1})]^{2+}$ (M = Mn, Co, or Ni) complexes.

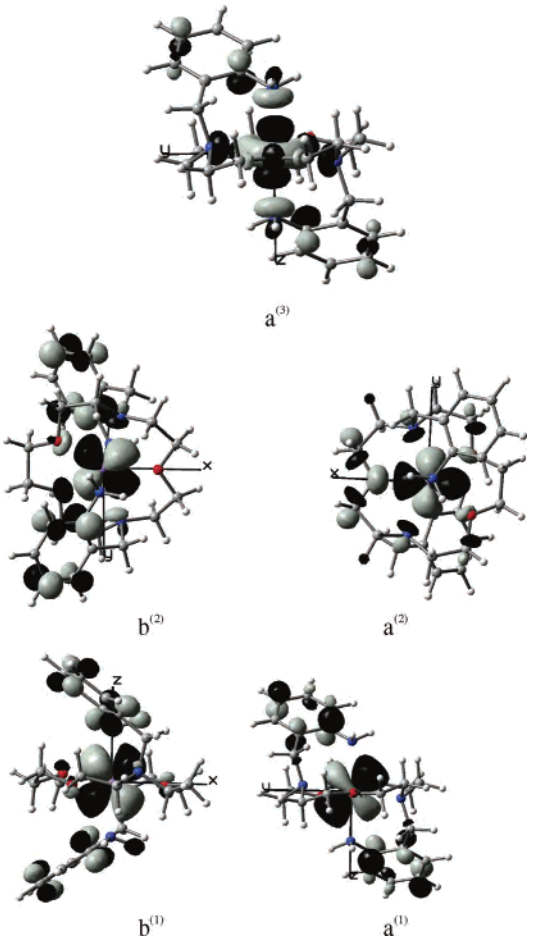

Figure 6. Surface plots of the Mn-based β MOs obtained from UB3LYP calculations for $[Mn(\mathbf{L^1})]^{2+}$.

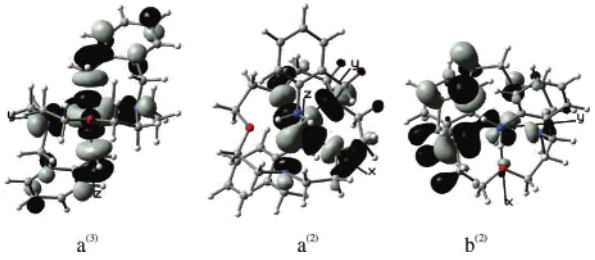

Figure 7. Surface plots of selected Ni-based β MOs obtained from DFT calculations for $[Ni(\mathbf{L^1})]^{2+}$.

metal d_{xy} and $d_{x^2-y^2}$ contribution, which is consistent with a Jahn−Teller effect. This distortion results in a C_1 symmetry for $[Ni(\mathbf{L^1})]^{2+}$ even when all d orbitals (except d_{xz} and d_{yz}) belong to the same symmetry species in the C_2 point group, and therefore they can mix and lose near-degeneracy within the C_2 point group with no need to distort to C_1 symmetry.

Surface plots of calculated $a^{(3)}$, $a^{(2)}$, and $b^{(2)}$ β spin MOs for $[Ni(\mathbf{L^1})]^{2+}$ are shown in Figure 7. The occupied $b^{(2)}$ MO also possesses antibonding character with respect to the interaction between the metal and donor atoms of the macrocyclic ring. The occupation of this antibonding orbital weakens certain metal−donor bonds. Indeed, $b^{(2)}$ possesses a strong antibonding character with respect to the interaction with O(1) and N(1) (Figure 7), which results in the lengthening of the calculated Ni−O(1) and Ni−N(1) bond distances (Table 2). Thus, the qualitative picture of the MO diagrams presented here predicts a binding strength of $\mathbf{L^1}$ to Ni(II) that is weaker than that to Mn(II) and Co(II) because of the occupation of MO with antibonding character, whereas the binding strengths of $\mathbf{L^1}$ to Mn(II) and Co(II) are expected to be similar.

Stability of the Complexes in Solution. Our electronic structure studies described above predict that the binding strength of $\mathbf{L^1}$ to Mn(II), Co(II), and Ni(II) ions should follow the following trend: Co(II) ≈ Mn(II) > Ni(II). To check if this is reflected in the stability of the complexes in solution, we performed spectrophotometric titrations of a solution of $\mathbf{L^1}$ with Mn(II), Co(II), and Ni(II) perchlorates in acetonitrile solution. The UV−vis spectrum of $\mathbf{L^1}$ shows two bands at 240 and 290 nm (E_2 and B bands of the aromatic rings), resulting from the $\pi \rightarrow \pi^*$ and $n \rightarrow \pi^*$ transitions on the aromatic subunits of the ligand. Upon addition of the metal salt, both absorption bands shift toward shorter wavelengths as their intensity decreases. Figure 8 shows the spectral changes observed during the formation of the Ni(II) complex. Similar plots obtained for the Mn(II) and Co(II) complexes are given in the Supporting Information (Figures S1 and S2). In all cases, a 1:1 reaction stoichiometry was ascertained, as the data displayed a single inflection point when the M:ligand molar ratio was close to 1. The steep curvature of the titration profile corresponds to an especially high equilibrium constant (log K > 7). In particular, the p parameter (p = [concentration of complex]/[maximum possible concentration of complex]) was found in any case to be higher than 0.8, a condition which does not allow for the determination of a reliable equilibrium constant.[44] However, the spectral changes observed during the spectrophotometric

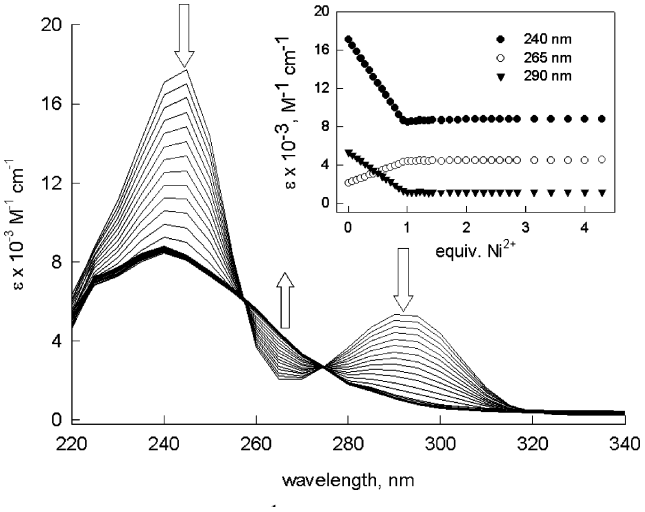

Figure 8. UV−vis spectrum of $\mathbf{L^1}$ in acetonitrile solution, and spectral changes upon addition of aliquots of a solution of $Ni(ClO_4)_2 \cdot 6H_2O$ in the same solvent.

titrations can be used to obtain a rough estimate of the strength of the coordination, which permits us to establish a qualitative stability sequence. Indeed, upon coordination to the metal ion, the electron density on the $-NH_2$ groups and aromatic units of $\mathbf{L^1}$ decreases. The probability of the electronic transition is related to the electron density of these groups: the lower the electron density, the lower the probability of the transition and the value of the molar absorbance. Thus, the relative molar absorbance variation of the band at 290 nm, $\Delta\epsilon_{r(290)}$, can be used to estimate the strength of the coordination of $\mathbf{L^1}$

$$\Delta\epsilon_{r(290)} = \frac{(\epsilon_{290}(\mathbf{L^1}) - \epsilon_{290}([M\mathbf{L^1})]^{2+})}{\epsilon_{290}(\mathbf{L^1})} \qquad (7)$$

where $\epsilon_{290}(\mathbf{L^1})$ and $\epsilon_{290}([M(\mathbf{L^1})]^{2+})$ are the molar absorbances at 290 nm of ligand $\mathbf{L^1}$ and the corresponding metal complex, respectively. We have obtained $\Delta\epsilon_{r(290)}$ values of 0.862 (Mn), 0.881 (Co), and 0.785 (Ni). These data therefore suggest the stability sequence for the complexes of $\mathbf{L^1}$ of Co(II) ≈ Mn(II) > Ni(II), in nice agreement with the qualitative predictions of our theoretical calculations.

(44) Wilcox, C. S. In *Frontiers in Supramolecular Chemistry and Photochemistry*; VCH: Weinheim, Germany, 1991; pp 123−143.

Conclusions

The lariat ether *N*,*N*′-bis(2-aminobenzyl)-1,10-diaza-15-crown-5 ($\mathbf{L^1}$) forms mononuclear complexes with Mn(II), Co(II), and Ni(II), where the metal ion is seven-coordinated in a distorted pentagonal bipyramidal geometry. The X-ray structures of the Mn(II) and Co(II) complexes show C_2 symmetries of the $[M(\mathbf{L^1})]^{2+}$ cations, whereas the structures of the Ni(II) complexes **5** and **6** show a more distorted coordination environment. Electronic structure calculations of the $[M(\mathbf{L^1})]^{2+}$ systems (M = Mn, Co, or Ni) predict a similar ordering of the metal-based frontier MOs for the Mn(II) and Co(II) complexes. The metal contribution to the first two β frontier MOs (labeled in terms of C_2 symmetry), $a^{(1)}$ and $b^{(1)}$, is primarily d_{yz} and d_{xz}, respectively. At somewhat higher energy are the pseudodegenerated $a^{(2)}$ and $b^{(2)}$ MOs, which possess $d_{x^2-y^2}$ and d_{xy} character. At highest energy are the $a^{(3)}$ orbitals, whose metal contribution is primarily d_{z^2}. This splitting of the metal-based β spin frontier MO leads to a pseudodegenerate ground state for the d^8 Ni(II) ion. The distortion of the coordination environment in $[Ni(\mathbf{L^1})]^{2+}$ is therefore consistent with a Jahn−Teller effect, which removes the pseudodegeneracy of the $a^{(2)}$ and $b^{(2)}$ MO. Our electronic structure calculations are consistent with the magnetic properties of the title compounds and predict that the binding strength of L^1 should follow the trend Co(II) ≈ Mn(II) > Ni(II), in agreement with the experimental data.

Acknowledgment. The authors thank Xunta de Galicia (PGIDIT03TAM10301PR) for generous financial support. The authors are indebted to Centro de Supercomputación de Galicia (CESGA) for providing the computer facilities. J.A.R. is grateful for financial support from the Spanish MEC-DGICYT through Project CTQ 2004-03456/BQU.

Supporting Information Available: X-ray crystallographic files, in CIF format, for compounds **1**, **3**, **5**, and **6**; Table S1 listing hydrogen-bonding geometry; Table S2 listing experimental and calculated angles of the metal coordination environment; Table S3 giving the difference between ideal and actual spin (spin contamination); Figures S1 and S2 showing the UV−vis spectra recorded during the titration of $\mathbf{L^1}$ with $Mn(ClO_4)_2 \cdot 6H_2O$ and $Co(ClO_4)_2 \cdot 6H_2O$; and in vacuo optimized geometries in *Z* matrix format (Å and deg) for the $[M(\mathbf{L^1})]^{2+}$ systems (M = Mn, Co, or Ni) in HS, LS, and IS configurations. This material is available free of charge via the Internet at http://pubs.acs.org.

IC051119H